frontiers | Frontiers in Sustainable Food Systems

TYPE Original Research
PUBLISHED 23 October 2024
DOI 10.3389/fsufs.2024.1448421

OPEN ACCESS

EDITED BY
Xixia Liu,
Hubei Normal University, China

REVIEWED BY
Nan Hao,
Nanjing University of Information Science and Technology, China
Ding Jiang,
Changzhou University, China
Selvakumar Palanisamy,
Khalifa University, United Arab Emirates

*CORRESPONDENCE
Guoxin Ma
mgx@ujs.edu.cn
Qian Liu
liuqian@ujs.edu.cn

RECEIVED 13 June 2024
ACCEPTED 08 October 2024
PUBLISHED 23 October 2024

CITATION
Ma G, Shi Q, Hou X, Peng Y and Liu Q (2024) An electrochemical sensor for simultaneous voltammetric detection of ascorbic acid and dopamine enabled by higher electrocatalytic activity of co-modified MCM-41 mesoporous molecular sieve.
Front. Sustain. Food Syst. 8:1448421.
doi: 10.3389/fsufs.2024.1448421

An electrochemical sensor for simultaneous voltammetric detection of ascorbic acid and dopamine enabled by higher electrocatalytic activity of co-modified MCM-41 mesoporous molecular sieve

Guoxin Ma[1]*, Qiang Shi[2], Xiuli Hou[1], Yuxin Peng[1] and Qian Liu[1]*

[1]School of Agricultural Engineering, Jiangsu University, Key laboratory of Modern Agricultural Equipment and Technology (Ministry of Education), Zhenjiang, China, [2]School of Science and Technology, Shanghai Open University, Shanghai, China

It is of great value to develop effective methods for accurately and simultaneously detecting ascorbic acid (AA) and dopamine (DA) in the field of biochemistry. This work reports a nonenzymatic electrochemical sensor for the simultaneous detection of AA and DA by employing a Co-modified MCM-41 (CoMCM-41) mesoporous molecular sieve as an efficient electrocatalytic material, which was synthesized by a two-step hydrothermal method. Subsequently, the high structural organization of the CoMCM-41 mesoporous structure was characterized, and the electrocatalytic performance of CoMCM-41 toward AA and DA oxidation was then evidenced by the catalytic effect of different electrodes modified with or without CoMCM-41. By virtue of the superior electrocatalytic activity of the CoMCM-41, a much wider peak potential difference (ΔE_{pa}) of 310 mV was obtained for the oxidation of AA and DA in their mixture solution, and the parameters that influenced the electrochemical signals of the modified electrode were also optimized. Under optimal conditions, a good linear response to AA and DA was observed on the CoMCM-41 modified electrode. For individual detection of AA and DA, the linear ranges were 7 ~ 105 μM and 5 ~ 110 μM respectively, while the linear response range was 20 ~ 100 μM for simultaneous detection of AA and DA. Satisfactory recovery results were obtained when the fabricated sensor was applied to determine AA in orange juice and DA in madopar pill samples.

KEYWORDS

electrochemical sensor, simultaneous detection, ascorbic acid, dopamine, mesoporous molecular sieve

1 Introduction

Electrochemically active biomolecules such as dopamine (DA) and ascorbic acid (AA) are important biomedical compounds that play a crucial role in the human metabolism process (Liang et al., 2023). Dopamine, the most significant catecholamine, is an important neurotransmitter widely distributed in the brain for message transfer in the mammalian central nervous system. Dysfunctions of the dopaminergic system are related to neurological disorders such as schizophrenia, Parkinson's disease, and so forth (Li et al., 2021; Xia et al.,

2023). Ascorbic acid, also known as vitamin C, is an important water-soluble cytosolic chain-breaking antioxidant in the mammalian brain. In the presence of several neurotransmitter amines, including DA, AA has been used to prevent and treat the common cold, mental illness, and cancer (Yang et al., 2023; Xu et al., 2021). Considering the vital functions of biomolecules mentioned above, it is essential to develop practical methods to accurately and rapidly detect DA and AA in neurochemistry and biochemistry fields. Because of their analogous properties, selective and simultaneous DA and AA determination has attracted much attention in biomedical chemistry and diagnostic research.

Numerous efficient methods, including colorimetry (Hao et al., 2023), chemometric-assisted kinetic spectrophotometry (Moghadam et al., 2011), and ultraviolet–visible spectrophotometry (El-Zohry and Hashem, 2013), have been developed in past years for the determination of DA and AA. Compared with those methods, electrochemical sensing has the merits of simple operation, low cost, high sensitivity, and rapid response (Zhang et al., 2020). However, DA and AA have similar electrochemical properties on bare electrodes, which complicate the identification of their oxidation potential. Also, the overlap of their volt–ampere responses could hinder their simultaneous determination (Peng et al., 2022). To overcome those shortcomings, various outstanding functionalized nanomaterials, including noble metal/alloy nanoparticles (Demirkan et al., 2020; Yang et al., 2019), polymers (Li et al., 2020; Zhang et al., 2020), and carbon-based materials (Zhao et al., 2019; Arya Nair et al., 2022; Han et al., 2024) have been introduced as modifying materials. Mesoporous molecular sieves have been vigorously pursued since ExxonMobil introduced M41S materials in 1992 (Beck et al., 1992; Kresge et al., 1992). Due to their unique pore structure and large specific surface area, silica-based mesoporous materials are very attractive and convenient for immobilizing different catalysts in various electrocatalytic fields ranging from oxygen reduction and biomass oxidation to electrochemical sensing (Chen et al., 2013; Zhang et al., 2017; Terra et al., 2019; Feng et al., 2019; Zablocka et al., 2019). Mobil composition of matter No. 41 (MCM-41) is a promising candidate for a silica-based catalyst and catalyst support for electrochemical sensors due to its hexagonally arranged uniform pore structure and high thermal stability (Jin et al., 2017). Nevertheless, most of those silica-based materials are electronic insulators, and incorporating an additional material, such as noble metal nanoparticles (Iminova et al., 2015), semiconductor quantum dots (Pabbi and Mittal, 2017), and carbon-based materials (Abraham et al., 2015) is commonly required to improve the charge transfer efficiency of silica-based materials for electrochemical applications (Eguílaz et al., 2018). A previous report found that the catalytic efficiency of MCM-41 was improved by heteroatom loading (Hassan et al., 2017), which provided a novel candidate catalyst for fabricating electrochemical sensors with good performance. The incorporation of metallic ions such as V, Fe and Co in the network structure of MCM-41 molecular sieves has showed good results for the oxidation of organic molecules (Cánepa et al., 2017), however, few studies have been reported the use of such mesoporous materials modified with transition metal of Co in the oxidation and simultaneous detection of biomedical compounds of AA and DA.

In the present study, an effective electrochemical sensor for simultaneous detection of AA and DA was developed by using Co-modified MCM-41 (CoMCM-41) as the electrocatalytic material (Scheme 1). X-ray diffraction (XRD) analysis, transmission electron microscopy (TEM) and scanning electron microscopy (SEM) were used to characterize the as-prepared CoMCM-41 materials or CoMCM-41 based film. Then the electrochemical performance of the CoMCM-41 modified electrodes toward the oxidation of AA and DA were investigated by cyclic voltammetry (CV) and differential pulse voltammetry (DPV) techniques. The peak-to-peak separation potential between the oxidation peaks of AA and DA on CoMCM-41 modified electrodes was bigger enough for simultaneous detection of them. Finally, the electrochemical characteristics of CoMCM-41 modified electrodes for the individual and simultaneous detection of AA and DA were investigated by a DPV method. More importantly, real sample analysis was done by using the proposed CoMCM-41 based electrochemical sensing method.

2 Experimental

2.1 Chemicals and solutions

Sodium silicate ($Na_2SiO_3{\cdot}9H_2O$), sodium meta-aluminates ($NaAlO_2$), cobalt chlorate ($CoCl_2{\cdot}6H_2O$), cetyltrimethyl ammonium bromide (CTAB) were purchased from Shanghai Chemical Reagent Co., P. R. China. AA and DA were obtained from the Fourth Chemical Reagent Company of Shanghai and Sigma-Aldrich (United States), respectively. Phosphate-buffered saline (PBS, 0.1 M) solution of different pH were prepared by mixing stock solutions of NaH_2PO_4 and Na_2HPO_4, and then adjusted by H_3PO_4 or NaOH solution. Pill of madopar was obtained from Roche medical company (Shanghai). All of the chemicals were of analytical reagent grade and were used without further purification. All other aqueous solutions were prepared with deionized water.

2.2 Apparatus

XRD measurement was carried out with a Rigaku D Max 2500 PC X-ray diffractometer. Surface area and pore size distribution were measured using an NOVA2000 surface area and pore size analyzer from Quntachrome Corporation, the surface area was calculated with Brunauer–Emmett–Teller (BET) method and pore size distribution, pore volume was calculated with Barrett–Joyner–Halenda (BJH) method (Barrett et al., 1951). TEM image was taken with a JEOL 2100 TEM (JEOL, Japan) operated at 200 kV, and SEM was obtained with a JSM-6480 field-emission scanning electron microscope. All electrochemical experiments including CV and DPV were performed with a CHI660 electrochemical workstation (Chenhua, Shanghai, China). A conventional three-electrode electrochemical system was used for all electrochemical experiments, which consisted of a glassy carbon electrode (GCE) working electrode, a Pt wire auxiliary electrode and a saturated calomel reference electrode (SCE), respectively.

2.3 Synthesis of CoMCM-41

With some modifications, the CoMCM-41 mesoporous molecular sieves were synthesized by a reported two-step hydrothermal method

(Zhao et al., 2007). A composition of 2.13 g of $Na_2SiO_3 \cdot 9H_2O$, 0.12 g of $NaAlO_2$, and 1.43 g of $CoCl_2 \cdot 6H_2O$ was dissolved in 50 mL of deionized water and mixed with a H_2SO_4/deionized water solution (volume ratio 1:1) to adjust the pH value of the solution to equal 11.0. The gel was stirred for 3 h at 90°C, then transferred into a 100 mL Teflon-inner-container stainless steel water boiler and kept in an oven at 200°C for 5 h. The reaction mixture was cooled to room temperature and poured into another beaker containing 10.23 g of $Na_2SiO_3 \cdot 9H_2O$. The sample was stirred, creating the colloidal suspension liquid precursor (sample I). 4.85 g of CTAB was added to 25 mL water in another beaker, creating a transparent, glue-like suspension liquid (sample II). Sample I was slowly dropped into sample II with vigorous stirring, and the pH was adjusted to 11.0 using H_2SO_4 solution. After 1 h of stirring, the mixture was introduced to the boiler and kept in an oven at 130°C for 48 h. Finally, the CoMCM-41 was obtained after cooling, filtering, rinsing with deionized water, and drying at 120°C for 24 h.

2.4 Preparation of CoMCM-41 modified electrode

A bare GCE was polished successively with 1, 0.3, and 0.05 μm alumina slurries. Then, it was rinsed with doubly distilled water and sonicated in ethanol and doubly distilled water for 5 min. A suspension of CoMCM-41 (10 mg/mL) was obtained by dispersing 10 mg CoMCM-41 in 10 mL of a 0.2% chitosan (CHI) solution. 10 μL of CoMCM-41 suspension was dropped to cover the surface of the electrode, then the CoMCM-41 modified electrode (denoted as CoMCM–CHI/GCE) was kept at 4°C for 12 h to dry, then stored for further use. With the help of the CHI employed in the CoMCM–CHI/GCE, the CoMCM-41 particles could be embedded on the surface of electrode much easier and successfully.

3 Results and discussion

3.1 Characterization of CoMCM-41

Figure 1A shows XRD patterns of the as-prepared CoMCM-41 at small angles. As shown, the sample had a distinct diffraction peak at (100) at 2θ of 2.3°, showing the high structural organization of the mesoporous structure (Zhao et al., 2007). The adsorption–desorption isotherms and pore size distribution curves of the sample are shown in Figure 1B, which shows that the adsorption–desorption isotherms of the sample were typical type IVs, indicating its mesoporous framework (Beck et al., 1992). Adsorption and desorption isotherms of the sample were obviously abrupt in a relative pressure range of 0.4–0.6, demonstrating that CoMCM-41 had a mesoporous larger pore size, which was consistent with the pore size distribution curve of CoMCM-41 in Figure 1C. It can be clearly seen form the TEM image (Figure 1D) that the as-prepared CoMCM-41 exhibited a mesoporous structure (Zhao et al., 2007). These results above indicated the successfully synthesized of CoMCM-41 mesoporous material. By virtue of its electrocatalytic activity, CoMCM-41 was then used for construction a sensing platform toward electrochemically active biomolecules of AA and DA. After the modification of electrodes, SEM was employed to characterize the morphology of the CoMCM–CHI film on the surface of GCE. Figure 1E shows the surface image of a pure layer of CHI, which formed a flat and homogeneous film across the entire section. However, after the CoMCM-41 particles were embedded by CHI on the electrode surface, the rugged appearance was observed obviously for the CoMCM–CHI film (Figure 1F), which indicated the successful modification of the CoMCM–CHI/GCE.

3.2 CV behavior of AA and DA on the modified electrode

Figure 2A illustrates the CV responses of bare GCE, CHI/GCE, and CoMCM-CHI/GCE recorded in 0.1 M PBS (pH 4.0) in the presence of 120 μM AA. It can be seen that the AA showed an irreversible oxidation peak and a much smaller CV peak response on the bare GCE (curve a). The anodic peak current of AA at the CHI/GCE (curve b) showed no obvious change compared with the bare GCE, whereas at the CoMCM–CHI/GCE (curve c), the peak current of the AA was 2.3 times larger than that of the bare GCE, and the peak potential shifted more negatively. At the same time, the anodic peak current of DA at the bare GCE showed a small anodic peak with a peak potential of approximately 500 mV (curve a in Figure 2B). An observed change of anodic peak current and a peak potential shift of 90 mV was obtained at the CHI/GCE (curve b), whereas a 2.1 times larger anodic peak current compared to the bare GCE was observed at the CoMCM–CHI/GCE (curve c). Those phenomena are clear evidence of the catalytic effect of the chemically modified electrode toward the oxidation of AA and DA. The CV responses of CoMCM–CHI/GCE scanned under different scan rate from 10 to 100 mV/s was displayed in Figures 3A,C, and it can be clear seen that the peak currents of the electrode were increased gradually with the increasing of the scan rate. As shown in Figures 3B–D, the peak currents of the CoMCM–CHI/GCE for the oxidation of AA and DA were linearly proportional to the scan rates in the range of 10 ~ 100 mV/s, indicating an adsorption-controlled electrode process for the electro-oxidation of AA and DA at the CoMCM–CHI/GCE (Han et al., 2023).

3.3 Optimization of the experimental conditions

The concentration of CoMCM-41 at the peak current of DA was investigated firstly. As shown in Figure 4A, the peak current of AA increased with the increase in CoMCM-41 concentration from 4.0 to 8.0 mg/mL, and little change of the peak current was observed when the CoMCM-41 content exceeded 8.0 mg/mL. Figure 4B shows that the peak current of DA increased with the increase in CoMCM-41 concentration from 4.0 to 10.0 mg/mL. Because of the sensitivity of the current response, 10.0 mg/mL of CoMCM-41 gel was chosen for electrode modification in this work. The effect of the pH value of PBS on the oxidation potential of AA and DA was studied in the range of 2.0 to 8.0 (Figure 4C). As shown, the peak potential of AA (curve a) shifted negatively by 75 mV/pH with the increase in pH. When pH < 5.0, the minimum potential was at pH = 5.0, and the peak potential stayed constant when pH > 5.0. Although the peak potential of DA (curve b) was proportional to pH, it shifted negatively by 60 mV/pH

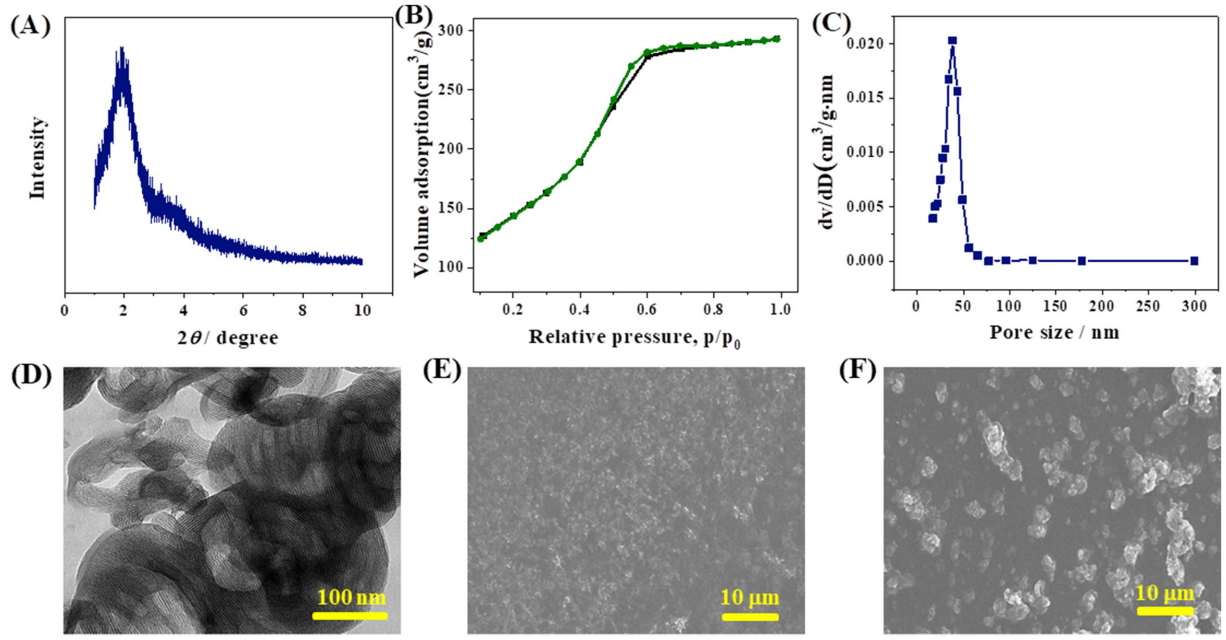

FIGURE 1
(A) XRD patterns of the as-prepared CoMCM-41; (B) adsorption and desorption isotherms of CoMCM-41; (C) the pore size distribution curve of CoMCM-41; (D) TEM image of CoMCM-41; SEM images of GCE modified with (E) 0.2% CHI and (F) CoMCM-41 dispersed in 0.2% CHI.

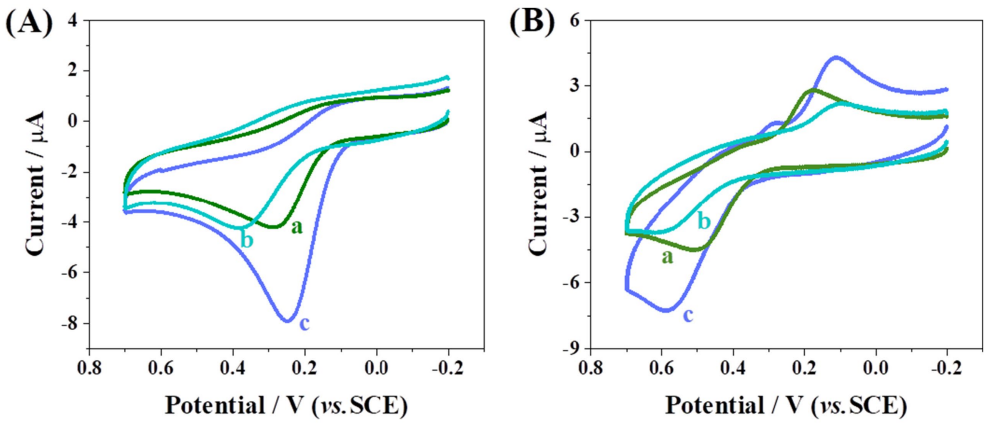

FIGURE 2
CV curves of bare GCE (a), CHI/GCE (b) and CoMCM-CHI/GCE (c) in 0.1 M PBS (pH 4.0) in the presence of 120 μM (A) AA and (B) DA, respectively.

with the increase in solution pH. Therefore, 0.1 M PBS with a pH of 4.0 was selected for the following experiment.

3.4 Oxidation of mixture of AA and DA at CoMCM-CHI/GCE

Ascorbic acid and DA always exist together in a biological environment, but simultaneous determination of AA and DA is difficult on a bare GCE and other solid electrodes. In this work, the peak potentials could be distinguished at the CoMCM–CHI/GCE. The CV behavior of an AA and DA mixed solution was studied on the bare GCE, the CHI/GCE, and the CoMCM–CHI/GCE. As shown in Figure 4D, the AA and DA showed 2 broad anodic peaks of 380 mV and 530 mV, respectively at the bare GCE (curve b). Only one overlapped peak (380 mV) was at the CHI/GCE (curve a). For the CoMCM–CHI/GCE, two well-defined peaks were observed at approximately 280 mV and 590 mV, corresponding to AA and DA oxidation, respectively, (curve c). The peak potential difference (ΔE_{pa}) between the oxidation of AA and DA reached 310 mV, which was attributed to the promoted adsorption of these molecules on the porous nanostructure of CoMCM-41 film with high surface area and these abundant active sites (Zhang et al., 2018; Peng et al., 2023). More importantly, the ΔE_{pa} of 310 mV obtained in this work was much bigger than those reported in the recent works listed in Table 1 (Peng et al., 2022; Yang et al., 2023; Celik Cogal et al., 2024; Jia et al., 2024; Darabi et al., 2023), indicating

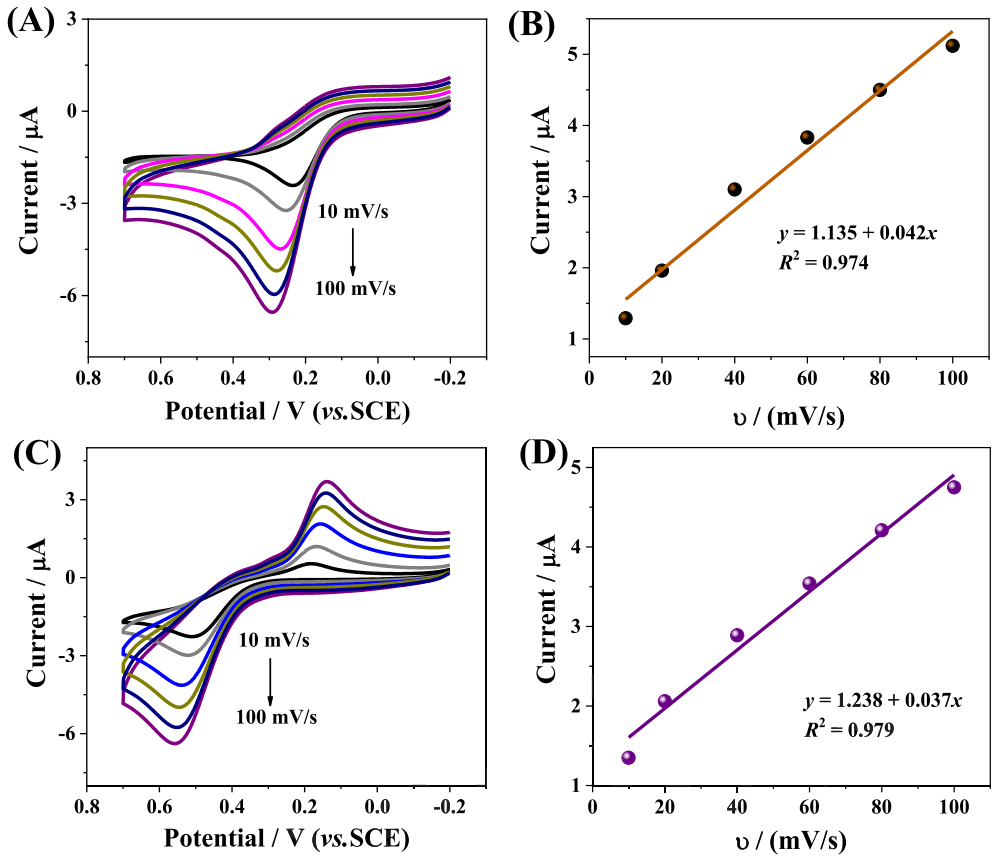

FIGURE 3
CV curves of CoMCM-CHI/GCE in 0.1 M PBS (pH 4.0) with 20 μM (A) AA and (C) DA at various scan rates of 10, 20, 40, 60, 80, and 100 mV/s. The corresponding plots of peak current versus scan rate for (B) AA and (D) DA, respectively.

the high catalytic oxidation activity of the proposed CoMCM–CHI/GCE for simultaneous determination of AA and DA.

3.5 Simultaneous determination of AA and DA

The electro-oxidation processes of AA and DA in the mixture were investigated by DPV when the concentration of one species changed while that of another species remained constant. Figure 5A gives the DPV recordings of the CoMCM–CHI/GCE with various DA concentrations in the presence of 100 μM of AA. As shown, the peak currents increased with the increasing of DA concentrations. The oxidation peak current was proportional to the DA concentration, and there was a linear relation between the oxidation peak currents of DA and its concentration over a range of 5 ~ 110 μM. The linear regression equation was I (μA) = 0.184 + 0.030C_{DA} (μM), R^2 = 0.985 (Figure 5B), and the limit of detection (LOD) was 1.7 μM (S/N = 3). Similarly, as shown in Figures 5C,D, the oxidation peak currents were proportional to the AA concentrations in the range of 7 ~ 105 μM with a LOD of 2.1 μM (S/N = 3). The linear regression equation was I (μA) = 0.138 + 0.404C_{AA} (μM), R^2 = 0.994. To demonstrate the analytical performance of the CoMCM–CHI based sensor, the linear response range and LOD were compared with previous reports in the literatures. As depicted in Table 1, the proposed sensor exhibited better or comparable performance toward AA and DA detection. Those results demonstrated that the CoMCM–CHI/GCE proposed in this work is a promising candidate for the simultaneous determination of AA and DA in a mixture without cross interference.

Subsequently, the DPV responses of the CoMCM–CHI/GCE recorded in 0.1 M PBS (pH 4.0) with various concentrations of the two species were also investigated. As depicted in Figure 6A, the electrochemical responses of the CoMCM–CHI/GCE were increased gradually with the increasing of the concentrations of the two species from 20 to 100 μM, respectively and the oxidation peak currents of AA and DA were clearly separated from each other, which indicated that the electrochemical detection of the two species can be resolved well from their mixed solutions, resulted in the high accuracy of the sensor from the mutual interference. Figure 6B indicates that the oxidation peak currents of CoMCM–CHI/GCE increased linearly with increasing concentrations of both AA and DA in the concentration range of 20 ~ 100 μM, which demonstrated that the proposed CoMCM-41 based electrochemical sensor was possible to discriminate and simultaneously detect AA and DA in their mixture solution by the conventional DPV method.

3.6 Real sample analysis

The CoMCM–CHI/GCE was applied to measure AA in orange juice using a standard addition method; the results are listed in

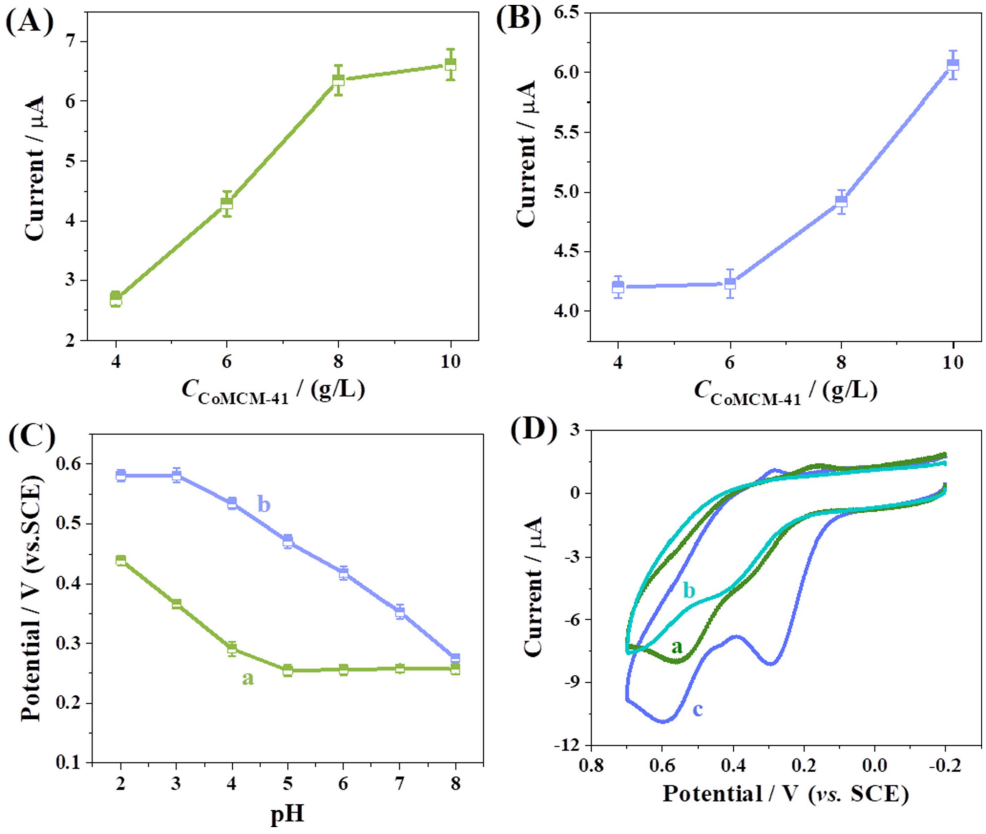

FIGURE 4
Effect of CoMCM-41 concentration on the peak current for the oxidation of (A) AA and (B) DA, (C) effect of pH value on the peak potential for the oxidation of AA (a) and DA (b); (D) CV curves for oxidation of AA (120 μM) and DA (120 μM) at bare GCE (a), CHI/GCE (b) and CoMCM-CHI/GCE (c) in 0.1 M PBS (pH 4.0).

TABLE 1 Comparison of ΔE_{pa} between AA and DA, CoMCM-CHI/GCE for AA and DA detection with different modified electrodes.

Modified electrodes	ΔE_p (V)	Linear range (μM)		LOD (μM)		References
		AA	DA	AA	DA	
3D-KSC/C_{CSBP}[a]/GCE	0.24	1,980–6,000	14.1–100	660	4.6	Peng et al. (2022)
PtCo/N-CNSs[b] electrode	0.19	30–1,900	0.5–80	1.02	0.12	Yang et al. (2023)
GCE-Co/$MoSe_2$/PPy@CNF[c]	0.16	30–3,212	1.2–536	6.32	0.45	Celik Cogal et al. (2024)
$Ti_3C_2T_x/TiO_2$ NWs[d]/GCE	0.14	300–1,800	2–9 and 9–33	6.61	0.093	Jia et al. (2024)
rGO/PPy-Pt[e]/GCE	0.19	800–2,100	30–1,400	0.12	0.071	Darabi et al. (2023)
CoMCM-CHI/GCE	0.31	7–105	5–110	2.1	1.7	This work

3D-KSC/C_{CSBP}[a]: N-doped carbon nanosheets/three-dimensional porous carbon.
PtCo/N-CNSs[b]: PtCo nanocrystals/porous N-doped carbon nanospheres.
PPy@CNF[c]: polypyrrole hybrid-based carbon nanofiber.
$Ti_3C_2T_x/TiO_2$ NWs[d]: $Ti_3C_2T_x/TiO_2$ nanowires.
rGO/PPy-Pt[e]: reduced graphene oxide/polypyrrole-platinum nanocomposite.

Table 2. As is shown, the recoveries and relative standard deviation for the determination of AA were in the ranges of 98.61–101.71% and 0.39–2.15%, respectively. That modified electrode was also applied to determine the recovery of a madopar pill in spiking DA using the standard addition method. One madopar pill was dispersed in 5 mL PBS to fit into the linear range of DA. The samples were diluted 12.5 times with PBS (pH 4.0) for detection. The diluted sample was spiked with various concentrations of DA, and its DPV could be obtained by the modified electrode. The recovery results are listed in Table 3. The recoveries and relative standard deviation for the determination of AA were in the ranges of 98.09–100.64% and 1.31–2.32%, respectively. Those recoveries and precisions were acceptable, showing that the modified electrode could be efficiently applied to determine AA and DA in real samples. Furthermore, to verify the reliability and accuracy

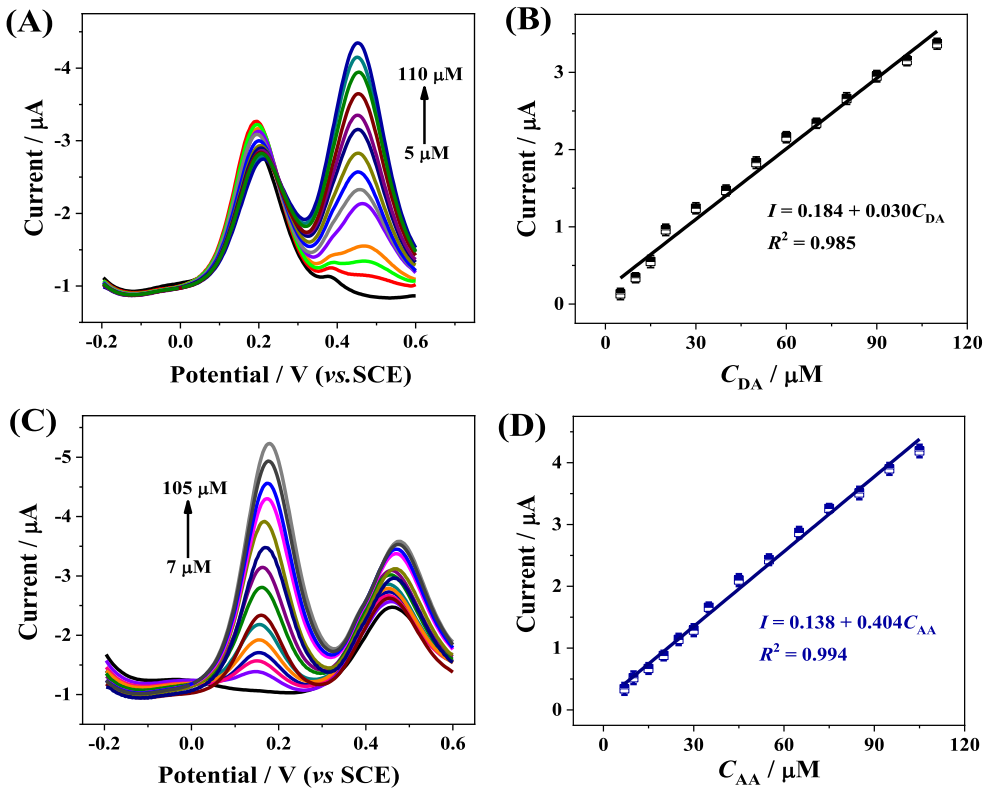

FIGURE 5
(A) DPV curves of CoMCM-CHI/GCE in 0.1 M PBS (pH 4.0) with different DA concentrations (from bottom to top: 0, 5, 10, 15, 20, 30, 40, 50, 60, 70, 80, 90, 100, 110 μM) in the presence of 100 μM AA, (B) the calibration plot for DA detection, (C) DPV curves of CoMCM-CHI/GCE in 0.1 M PBS (pH 4.0) with different AA concentrations (from bottom to top: 0, 7, 10, 15, 20, 25, 30, 35, 45, 55, 65, 75, 85, 95, 105 μM) in the presence of 100 μM DA, (D) the calibration plot for AA detection.

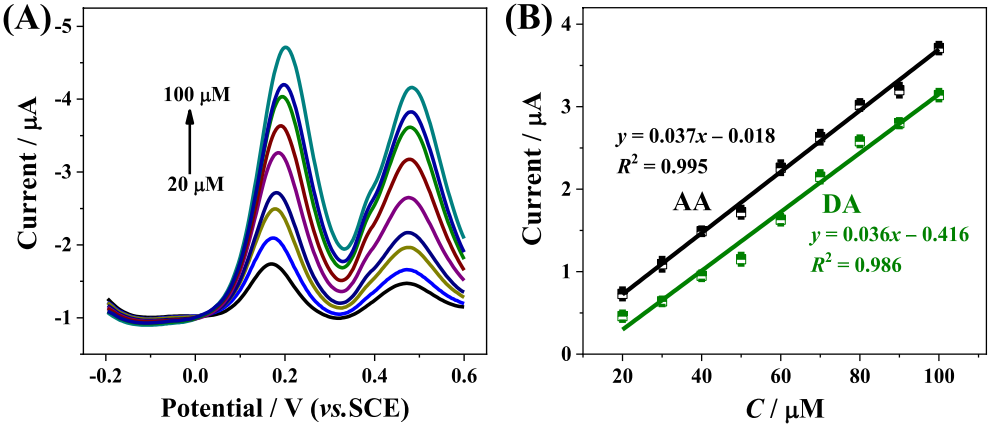

FIGURE 6
(A) DPV curves of CoMCM-CHI/GCE for simultaneous detection of AA and DA in 0.1 M PBS (pH 4.0) with their changed concentrations (20, 30, 40, 50, 60, 70, 80, 90, and 100 μM from bottom to top), (B) the calibration plots for simultaneous detection of AA and DA.

of the proposed electrochemical sensing method, high-performance liquid chromatography (HPLC) was applied to detect these spiked samples for comparison. The consistency between the two methods shown in Tables 2, 3 confirmed the accuracy of the proposed electrochemical sensor for AA and DA detection.

4 Conclusion

In summary, Co-containing mesoporous molecular sieves of CoMCM-41 were synthesized successfully by introducing Co-saponite into the pore wall. XRD characterization, adsorption–desorption

TABLE 2 Determination of AA in orange juice with the proposed electrochemical sensor and standard HPLC method ($n = 5$).

Samples	Electrochemical sensor					HPLC
	Detected (μM)	Added (μM)	Found (μM)	Recovery	RSD	Found (μM)
1	6.88	70.00	76.71	99.78%	0.39%	75.42
2	13.76	70.00	83.90	100.16%	1.28%	Not tested
3	20.64	70.00	90.18	99.49%	2.15%	Not tested
4	27.70	70.00	96.35	98.61%	1.73%	Not tested
5	34.62	70.00	106.41	101.71%	2.04%	103.35

TABLE 3 Determination of DA in madopar pills with the proposed electrochemical sensor and standard HPLC method ($n = 5$).

Samples	Electrochemical sensor					HPLC
	Detected (μM)	Added (μM)	Found (μM)	Recovery	RSD	Found (μM)
1	29.91	70.00	99.10	99.19%	1.47%	98.74
2	44.86	70.00	115.57	100.62%	2.32%	Not tested
3	59.81	70.00	130.64	100.64%	1.40%	Not tested
4	74.77	70.00	142.01	98.09%	1.31%	Not tested
5	89.72	70.00	158.88	99.47%	1.43%	156.36

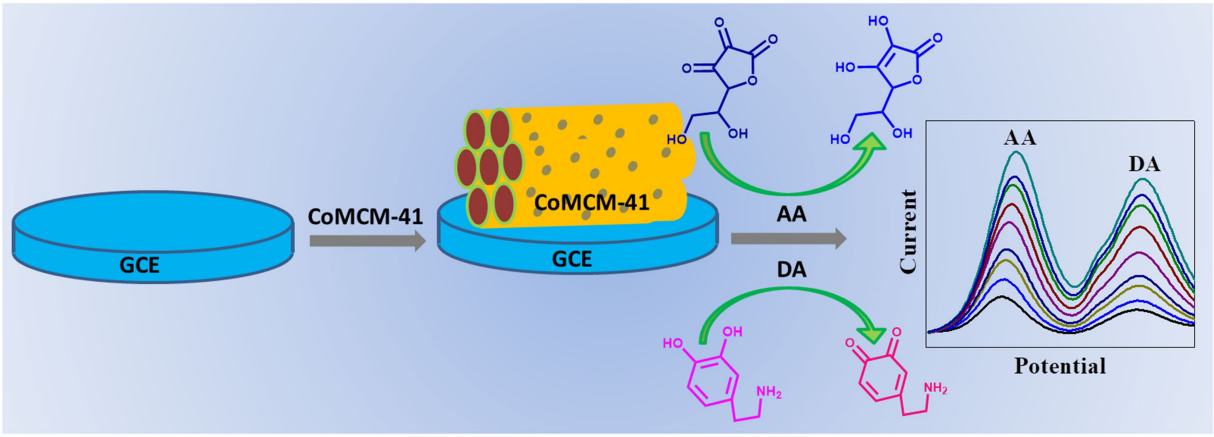

SCHEME 1
Schematic diagram for fabrication of CoMCM-41 based electrochemical sensor for simultaneous detection of AA and DA.

isotherms and pore size distribution curves indicated the high structural organization of the mesoporous structure. Employing the as-prepared CoMCM-41 as an ideal electrode modification material, the novel CoMCM–CHI/GCE had remarkable electrocatalytic activity for the oxidation of AA and DA simultaneously, and it needs to be emphasized that the proposed CoMCM–CHI/GCE showed a wider separation of peak currents between the oxidation of AA and DA. Good linear response to AA and DA was observed on the CoMCM-41 modified electrode, and satisfactory recovery results were obtained when the fabricated sensor was applied to determine AA in orange juice and DA in madopar pill samples. Those properties indicated that the CoMCM–CHI/GCE is promising for efficient AA and DA measurements in actual samples.

Data availability statement

The raw data supporting the conclusions of this article will be made available by the authors, without undue reservation.

Author contributions

GM: Data curation, Writing – review & editing. QS: Data curation, Writing – review & editing. XH: Writing – review & editing. YP: Writing – review & editing. QL: Supervision, Writing – original draft, Writing – review & editing.

Funding

The author(s) declare financial support was received for the research, authorship, and/or publication of this article. This work was supported by the Innovation/Entrepreneurship Program of Jiangsu Province and the Priority Academic Program Development of Jiangsu Higher Education Institutions (No. PAPD-2023-87), National Natural Science Foundation of China (No. 32201686), Postdoctoral Science Foundation of China (No. 2022M713499), Senior Talent Foundation of Jiangsu University (No. 19JDG026), and Postgraduate Research and Practice Innovation Program of Jiangsu Province (SJCX24_2423).

Conflict of interest

The authors declare that the research was conducted in the absence of any commercial or financial relationships that could be construed as a potential conflict of interest.

Publisher's note

All claims expressed in this article are solely those of the authors and do not necessarily represent those of their affiliated organizations, or those of the publisher, the editors and the reviewers. Any product that may be evaluated in this article, or claim that may be made by its manufacturer, is not guaranteed or endorsed by the publisher.

References

Abraham, S., Srivastava, S., Kumar, V., Pandey, S., Rastogi, K., Nirala, N. R., et al. (2015). Enhanced electrochemical biosensing efficiency of silica particles supported on partially reduced graphene oxide for sensitive detection of cholesterol. *J. Electroanal. Chem.* 757, 65–72. doi: 10.1016/j.jelechem.2015.09.016

Arya Nair, J. S., Saisree, S., Aswathi, R., and Sandhya, K. Y. (2022). Ultra-selective and real-time detection of dopamine using molybdenum disulphide decorated graphene-based electrochemical biosensor. *Sensors Actuators B Chem.* 354:131254. doi: 10.1016/j.snb.2021.131254

Barrett, E. P., Joyner, L. G., and Halenda, P. P. (1951). The determination of pore volume and area distributions in porous substances. I. Computations from nitrogen isotherms. *J. Am. Chem. Soc.* 73, 373–380. doi: 10.1021/ja01145a126

Beck, J. S., Vartuli, J. C., Roth, W. J., Leonowicz, M. E., Kresge, C. T., Schmitt, K. D., et al. (1992). A new family of mesoporous molecular sieves prepared with liquid crystal templates. *J. Am. Chem. Soc.* 114, 10834–10843. doi: 10.1021/ja00053a020

Cánepa, A. L., Elías, V. R., Vaschetti, V. M., Sabre, E. V., Eimer, G. A., and Casuscelli, S. G. (2017). Selective oxidation of benzyl alcohol through eco-friendly processes using mesoporous V-MCM-41, Fe-MCM-41 and co-MCM-41 materials. *Appl. Catal. A* 545, 72–78. doi: 10.1016/j.apcata.2017.07.039

Celik Cogal, G., Cogal, S., Machata, P., Uygun Oksuz, A., and Omastová, M. (2024). Electrospun cobalt-doped 2D-$MoSe_2$/polypyrrole hybrid-based carbon nanofibers as electrochemical sensing platforms. *Microchim. Acta* 191:75. doi: 10.1007/s00604-023-06078-2

Chen, P. K., Lai, N. C., Ho, C. H., Hu, Y. W., Lee, J. F., and Yang, C. M. (2013). New synthesis of MCM-48 sanospheres and facile replication to mesoporous platinum nanospheres as highly active electrocatalysts for the oxygen reduction reaction. *Chem. Mater.* 25, 4269–4277. doi: 10.1021/cm402349f

Darabi, R., Karimi-Maleh, H., Akin, M., Arikan, K., Zhang, Z., Bayat, R., et al. (2023). Simultaneous determination of ascorbic acid, dopamine, and uric acid with a highly selective and sensitive reduced graphene oxide/polypyrrole-platinum nanocomposite modified electrochemical sensor, and folic acid. *Electrochim. Acta* 457:142402. doi: 10.1016/j.electacta.2023.142402

Demirkan, B., Bozkurt, S., Cellat, K., Arıkan, K., Yılmaz, M., Şavk, A., et al. (2020). Palladium supported on polypyrrole/reduced graphene oxide nanoparticles for simultaneous biosensing application of ascorbic acid, dopamine, and uric acid. *Sci. Rep.* 10:2946. doi: 10.1038/s41598-020-59935-y

Eguílaz, M., Villalonga, R., and Rivas, G. (2018). Electrochemical biointerfaces based on carbon nanotubes-mesoporous silica hybrid material: bioelectrocatalysis of hemoglobin and biosensing applications. *Biosens. Bioelectron.* 111, 144–151. doi: 10.1016/j.bios.2018.04.004

El-Zohry, A. M., and Hashem, E. Y. (2013). Environmental method to determine dopamine and ascorbic acid simultaneously via derivative spectrophotometry. *J. Spectrosc.* 2013:260376. doi: 10.1155/2013/260376

Feng, Y. H., Li, W. L., Meng, M. J., Yin, H. B., and Mi, J. L. (2019). Mesoporous Sn(IV) doping MCM-41 supported Pd nanoparticles for enhanced selective catalytic oxidation of 1,2-propanediol to pyruvic acid. *Appl Catal B* 253, 111–120. doi: 10.1016/j.apcatb.2019.04.051

Han, E., Li, L., Gao, T., Pan, Y. Y., and Cai, J. R. (2024). Nitrite determination in food using electrochemical sensor based on self-assembled MWCNTs/AuNPs/poly-melamine nanocomposite. *Food Chem.* 437:137773. doi: 10.1016/j.foodchem.2023.137773

Han, E., Pan, Y. Y., Li, L., and Cai, J. R. (2023). Bisphenol a detection based on nano gold-doped molecular imprinting electrochemical sensor with enhanced sensitivity. *Food Chem.* 426:136608. doi: 10.1016/j.foodchem.2023.136608

Hao, P. P., Liu, Z. C., Wang, Z. W., Xie, M., and Liu, Q. Y. (2023). Colorimetric sensor arrays for antioxidant recognition based on Co_3O_4 dual-enzyme activities. *Analyst* 148, 3843–3850. doi: 10.1039/D3AN00939D

Hassan, H. M. A., Betiha, M. A., Elshaarawy, R. F. M., and Samy El-Shall, M. (2017). Promotion effect of palladium on Co_3O_4 incorporated within mesoporous MCM-41 silica for CO oxidation. *Appl. Surf. Sci.* 402, 99–107. doi: 10.1016/j.apsusc.2017.01.061

Iminova, Y. V., Tananaiko, O. Y., Rozhanchuk, T. S., Gruzina, T. G., Reznichenko, L. S., Malysheva, M. L., et al. (2015). Electrodes modified by a biocomposite film based on silica and gold nanoparticles for the determination of glucose. *J. Anal. Chem.* 70, 1247–1253. doi: 10.1134/S1061934815080109

Jia, D. Z., Yang, T., Wang, K., Zhou, L. L., Wang, E. H., Chou, K. C., et al. (2024). Facile in-situ synthesis of $Ti_3C_2T_x/TiO_2$ nanowires toward simultaneous determination of ascorbic acid, dopamine and uric acid. *J. Alloys Compd.* 985:173392. doi: 10.1016/j.jallcom.2023.173392

Jin, T., Yuan, W. H., Xue, Y. J., Wei, H., Zhang, C. Y., and Li, K. B. (2017). Co-modified MCM-41 as an effective adsorbent for levofloxacin removal from aqueous solution: optimization of process parameters, isotherm, and thermodynamic studies. *Environ. Sci. Pollut. Res.* 24, 5238–5248. doi: 10.1007/s11356-016-8262-0

Kresge, C. T., Leonowicz, M. E., Roth, W. J., Vartuli, J. C., and Beck, J. S. (1992). Ordered mesoporous molecular sieves synthesized by a liquid-crystal template mechanism. *Nature* 359, 710–712. doi: 10.1038/359710a0

Li, D. D., Liu, M., Zhan, Y. Z., Su, Q., Zhang, Y. M., and Zhang, D. D. (2020). Electrodeposited poly(3,4-ethylenedioxythiophene) doped with graphene oxide for the simultaneous voltammetric determination of ascorbic acid, dopamine and uric acid. *Microchim. Acta* 187:94. doi: 10.1007/s00604-019-4083-4

Li, Z. H., Zhang, X., Huang, X. W., Zou, X. B., Shi, J. Y., Xu, Y. W., et al. (2021). Hypha-templated synthesis of carbon/ZnO microfiber for dopamine sensing in pork. *Food Chem.* 335:127646. doi: 10.1016/j.foodchem.2020.127646

Liang, X. H., Yu, A. X., Bo, X. J., Du, D. Y., and Su, Z. M. (2023). Metal/covalent-organic frameworks-based electrochemical sensors for the detection of ascorbic acid, dopamine and uric acid. *Coordin. Chem. Rev.* 497:215427. doi: 10.1016/j.ccr.2023.215427

Moghadam, M. R., Dadfarnia, S., Haji Shabani, A. M., and Shahbazikhah, P. (2011). Chemometric-assisted kinetic–spectrophotometric method for simultaneous determination of ascorbic acid, uric acid, and dopamine. *Anal. Biochem.* 410, 289–295. doi: 10.1016/j.ab.2010.11.007

Pabbi, M., and Mittal, S. K. (2017). Electrochemical algal biosensor based on silica coated ZnO quantum dots for selective determination of acephate. *Anal. Methods* 9, 1672–1680. doi: 10.1039/C7AY00111H

Peng, W. J., Cai, L. X., Lu, Y. N., and Zhang, Y. Y. (2023). Preparation of Mn-co-MCM-41 molecular sieve with thermosensitive template and its degradation performance for rhodamine B. *Catalysts* 13:991. doi: 10.3390/catal13060991

Peng, X., Xie, Y., Du, Y., Song, Y. H., and Chen, S. H. (2022). Ultra-selective and real-time detection of dopamine using molybdenum disulphide decorated graphene-based electrochemical biosensor. *J. Electroanal. Chem.* 904:115850. doi: 10.1016/j.jelechem.2021.115850

Terra, J. C. S., Moores, A., and Moura, F. C. C. (2019). Amine-functionalized mesoporous silica as a support for on-demand release of copper in the a(3)-coupling reaction: ultralow concentration catalysis and confinement effect. *ACS Sustain. Chem. Eng.* 7, 8696–8705. doi: 10.1021/acssuschemeng.9b00576

Xia, Y. H., Li, G. L., Zhu, Y. F., He, Q. G., and Hu, C. P. (2023). Facile preparation of metal-free graphitic-like carbon nitride/graphene oxide composite for simultaneous determination of uric acid and dopamine. *Microchem. J.* 190:108726. doi: 10.1016/j.microc.2023.108726

Xu, X. C., Luo, Z. J., Ye, K., Zou, X. B., Niu, X. H., and Pan, J. M. (2021). One-pot construction of acid phosphatase and hemin loaded multifunctional metal–organic framework nanosheets for ratiometric fluorescent arsenate sensing. *J. Hazar. Mater.* 412:124407. doi: 10.1016/j.jhazmat.2020.124407

Yang, L., Wang, A. J., Weng, X. X., and Feng, J. J. (2023). Well-dispersed strawberry-like PtCo nanocrystals/porous N-doped carbon nanospheres for multiplexed assays. *Microchem. J.* 187:108421. doi: 10.1016/j.microc.2023.108421

Yang, H., Zhao, J., Qiu, M. J., Sun, P., Han, D. X., Niu, L., et al. (2019). Hierarchical bi-continuous Pt decorated nanoporous au-Sn alloy on carbon fiber paper for ascorbic acid, dopamine and uric acid simultaneous sensing. *Biosens. Bioelectron.* 124-125, 191–198. doi: 10.1016/j.bios.2018.10.012

Zablocka, I., Wysocka-Zolopa, M., and Winkler, K. (2019). Electrochemical detection of dopamine at a gold electrode modified with a polypyrrole-mesoporous silica molecular sieves (MCM-48) film. *Int. J. Mol. Sci.* 20:111. doi: 10.3390/ijms20010111

Zhang, W. J., Liu, L., Li, Y. G., Wang, D. Y., Ma, H., Ren, H. L., et al. (2018). Electrochemical sensing platform based on the biomass-derived microporous carbons for simultaneous determination of ascorbic acid, dopamine, and uric acid. *Biosens. Bioelectron.* 121, 96–103. doi: 10.1016/j.bios.2018.08.043

Zhang, Z. X., Liu, Y., Meng, W. J., Wang, J., Li, W., Wang, H., et al. (2017). One-pot synthesis of Ni nanoparticle/ordered mesoporous carbon composite electrode materials for electrocatalytic reduction of aromatic ketones. *Nanoscale* 9, 17807–17813. doi: 10.1039/C7NR06602C

Zhang, S., Xu, F., Liu, Z. Q., Chen, Y. S., and Luo, Y. L. (2020). Novel electrochemical sensors from poly [N-(ferrocenyl formacyl) pyrrole]@multi-walled carbon nanotubes nanocomposites for simultaneous determination of ascorbic acid, dopamine and uric acid. *Nanotechnology* 31:085503. doi: 10.1088/1361-6528/ab53bb

Zhang, X. N., Zhu, M. C., Jiang, Y. J., Wang, X., Guo, Z. M., Shi, J. Y., et al. (2020). Simple electrochemical sensing for mercury ions in dairy product using optimal Cu^{2+}-based metal-organic frameworks as signal reporting. *J. Hazar. Mater.* 400:123222. doi: 10.1016/j.jhazmat.2020.123222

Zhao, Q., Chu, J. Y., Jiang, T. S., and Yin, H. B. (2007). Synthesis and stability of CoMCM-41 mesoporous molecular sieve using cetyltrimethyl ammonium bromide as a template by two-step hydrothermal method, colloids and surfaces a: Physicochem. *Eng. Aspects* 301, 388–393. doi: 10.1016/j.colsurfa.2007.01.002

Zhao, Y. N., Zhou, J., Jia, Z. M., Huo, D. Q., Liu, Q. Y., Zhong, D. Q., et al. (2019). In-situ growth of gold nanoparticles on a 3D-network consisting of a MoS_2/rGO nanocomposite for simultaneous voltammetric determination of ascorbic acid, dopamine and uric acid. *Microchim. Acta* 186:92. doi: 10.1007/s00604-018-3222-7